Engineering Failure Analysis 138 (2022) 106323

Contents lists available at ScienceDirect

Engineering Failure Analysis

journal homepage: www.elsevier.com/locate/engfailanal

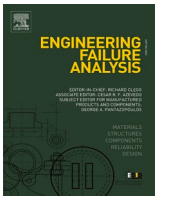

A design approach for controlled blade-off in overspeeding turbines

Ibrahim Eryilmaz [*,1], Vassilios Pachidis

Centre for Propulsion Engineering, School of Aerospace, Transport and Manufacturing, Cranfield University, Bedford MK430AL, UK

ARTICLE INFO

Keywords:
Turbine overspeed
Blade-off
LS-DYNA
Firtree

ABSTRACT

Following a shaft failure or loss of load in a gas turbine engine, the turbine overspeeds due to the continuing expansion through the stage(s). The overspeed may result in hazardous conditions which have to be prevented. Several mitigation methods include the control system's response by shutting the fuel flow, mechanical friction to reduce turbine acceleration, and blade release at a predetermined rotational speed. The release of the blades not only terminates the gas torque which accelerates the disk, but also increases the disk burst speed at reduced centrifugal load. In this manuscript, a design space exploration is presented to avoid disk burst by blade-off in a civil large turbofan engine through a parametric design of blade firtree and disk post system. The firtree design parameters used in the study are the contact angle between the blade firtree and the disk post, firtree bottom flank angle, firtree flank length and firtree thickness with respect to the disk post. The LS-DYNA finite element software was used in the simulations to generate possible failure scenarios. These were 'disk burst' and 'blade-off'. Blade-off conditions manifested in two ways as a function of design parameters. The first type was blade release from serrations without disk post failure, and the second type was blade escape with disk post failure. Following the design space exploration, the effect of several design and material parameters on the design space was investigated. These parameters are; the contact friction coefficient between the blade firtree and disk post, firtree serration number, and the strain hardening behavior of the material.

Introduction

Turbine overspeed is a common condition in gas turbine engines which is a result of the turbine loss of load (propeller or rotor pitch change) during rapid maneuvers. The magnitude of the overspeed in this case is in the order of 3–5% and is managed through fuel shut-off by the overspeed governors. On the other hand, turbine overspeed caused by a gas turbine shaft rupture is rare. During this rare condition, the overspeeding turbine rotor is subjected to excessive centrifugal loading and may fracture upon exceeding a certain limit. Aero-engines are certified on the basis that the outcome is non-hazardous. For the conditions where the outcome is hazardous, i.e. disk burst or uncontained blade-off, it must be shown that the probability of occurrence is extremely remote. This requires a good understanding of the design features, material properties and analysis techniques. This understanding also prevents extremely remote conditions becoming the sizing factor of the system design [9,10].

In Fig. 1 (a-b) describes the overspeed phenomenon followed by a shaft break. The failure position is assumed to be the drive arm

* Corresponding author.
E-mail address: ibrahimerylmz@yahoo.com (I. Eryilmaz).
[1] Current affiliation: Tusas Engine Industries Inc, Cevre Yolu, No:356, Eskisehir, Turkey.

https://doi.org/10.1016/j.engfailanal.2022.106323
Received 14 November 2021; Received in revised form 6 March 2022; Accepted 10 April 2022
Available online 18 April 2022

Nomenclature

A	Stress parameter
B	Strain hardening parameter
C	Contact point
c	Strain rate parameter
F	Force
L	Length
m	Thermal exponent
n	Strain hardening exponent
R	Recess
P	Protrusion
T	Temperature
t	Time
α	Flank angle at neutral state
β	Flank angle at rotated state
ΔP	Pressure difference
θ	Half contact angle
ε	Strain
$\dot{\varepsilon}$	Strain rate
μ	Friction coefficient
σ	Stress

connecting the turbine and the compressor. Following the failure, the high-pressure gas in the upstream sections continues to be expanded and the gas torque accelerates the rotor. The pressure differential (ΔP) creates an end load pushing the rotor assembly in the downstream direction. The roller bearing in Fig. 1-a allows the turbine to dislocate, making it an 'unlocated' failure. Under the same conditions, the ball bearing in Fig. 1-b restricts the dislocation of the rotor. Therefore, this failure is called a 'located' failure.

The first prevention mechanism is the fuel shut-off, however, due to the permanent loss of turbine load, several other measures can be implemented. These are mechanical in nature and include friction to reduce acceleration, partial or complete blade destruction to cease gas torque, and increasing the burst limit depending on the severity of the case.

With the dislocation, the rotor comes into contact with the stationary structures behind it. These contacts (C) create an axial friction acting against the gas torque. Based on a methodology reported by Eryilmaz and Pachidis[6], the total frictional torque generated in the blade shank, disk rim, disk web and the bearing sections can be in the range of 20 to 50% of the gas torque depending on the number and the position of the contacts (Fig. 1-c). Here the rapid increase in the frictional torque at time unit 1.5 indicates the start of the blade to vane interaction which is called tangling. This phenomenon is an example of a mechanical prevention method in unlocated failures [12,13,4]. Additional to the fictional capacity, part-span blade failures can increase the tip clearance, degrade turbine performance and hence reduce gas torque [27,14].

For a given gas torque, the rotor speed during an unlocated failure can be up to 20% lower, with respect to a located failure (Fig. 1-c). Although the axial friction creates a significant advantage in reducing the acceleration, it relies on the turbine end load which may reverse direction with the accumulation of the high-pressure gas in the downstream reservoirs. In the given assembly, this scenario becomes possible with the closure of the disk rim and the disk web ports forming a closed cavity just after the rotor dislocation. In this

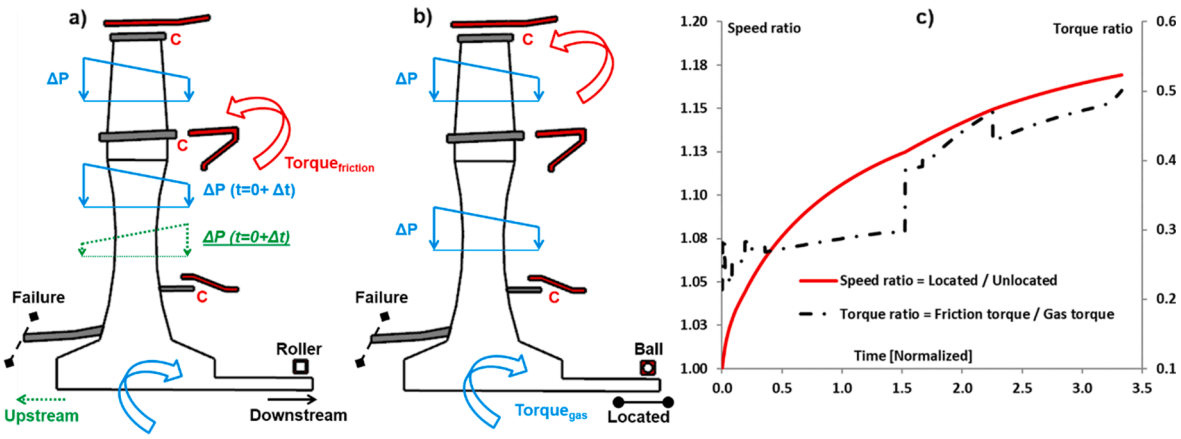

Fig. 1. a-b) Unlocated and located turbine assemblies and c) Speed and torque ratios for overspeed scenarios.

case, the pressure differential reverses direction, and the rotor instantaneously moves (Fig. 1-a, $t = 0 + \Delta t$) in the upstream direction terminating any frictional contacts [7].

Another form of frictional contact may occur in the radial direction. In the figure, the contacts at the disk web and the blade tip have this possibility, but this is subject to the presence of radial growth and unbalance. The radial growth is not only a variable among different materials but also depends on the heat treatment of the same material. For example, the ductility which can be associated with the radial growth can be higher in an annealed material than an aged one [28]. Depending on the magnitude of unbalance, partial or full rubs, including impacts between the rotor and the casing, can occur creating considerable amount of friction at high radius [16,37]. However, it should be noted that the unbalance can trigger secondary failures in the engine. It is known that a Boeing 737–217 sustained an engine power loss with fire during a Canadian North airline landing in 2008. In this case, one of the Pratt & Whitney 32JT8D-17A engine shafts failed due to an unbalance triggering rubbing (TSB 2008) [34]. Although the rubbing was initially associated with a bearing failure of one shaft, this led to the failure of the other shaft during the unbalanced motion.

1.1. Blade-off in turbines

Beyond the very first method, which is the fast detection and the immediate fuel shut-off for both located and the unlocated failures, axial friction is a natural way of overspeed prevention for the unlocated case. Considering the chaotic nature of the radial friction, which is prone to cause secondary failures, engine manufacturers apply another type of mechanical prevention method. This method is called 'blade shedding' which can be considered as a controlled blade-off and can be applied to both located and unlocated scenarios.

Soupizon [30] proposed an overspeed limiting arrangement to release the blades of a low-pressure turbine. In this method for the unlocated failures, the blades are intended to be cut from the struts as they came into contact with the static elements behind the rotor. The thick oversized static elements have a saw tooth shape in the region of contact to improve the cutting. Similarly, the Honeywell air turbine starter used in the General Electric CF6 engine has cutter ring structures that are located downstream of the air starter turbine disk. In an incident in 2007, the starter shaft failed in an unlocated manner on an Airbus A330-300 while on ground [2]. With the downstream movement, the blades were cut off from the disk. The disk was secured; however, the blades penetrated the containment ring and damaged nearby locations. Later, it was reported that the air starter was renewed to ensure the blade containment [1].

Lecuyer [19] proposed a round dimple on the pressure side of a Snecma low pressure turbine to initiate fracture of the blade at a predetermined speed of rotation. In this design, the dimple is positioned between 0% and 23% span from root at the pressure side of the blade having a 39% of the local thickness. During rotation above nominal speed, the locally increased stresses at the dimple region trigger the blade failure at a 10% lower speed than the disk fracture speed. Different from the previous two examples, the turbine does not need to be unlocated in this case, and the solution can also be applied to located failures.

For the same purpose where the turbine is located, a different design is applied in a Turbomeca engine. A Eurocopter AS-350 helicopter powered by a single Turbomeca Ariel 2B turboshaft engine experienced an engine compartment explosion during take-off in 2014. The reason of the explosion could not be determined due to extensive fire damage [23]. It was identified that the engine experienced foreign object damage. Both axial and centrifugal compressor blades were damaged and as the event progressed, the power turbine (free turbine) overspeeded. It was found that the turbine blades were separated from the disk at the overspeed notch located in the blade roots and they were contained by the casing shield. The blades featured a notch to trigger blade failure around 140–150% of free turbine speed (N2) to prevent disk from bursting around 170 % N2.

Herran et al.[15]modelled the transient engine mounting loads in unbalance conditions after blade shedding with explicit finite element simulations using the Europlexus software. The study is related to the overspeed protection system used in Turbomeca turboshaft engines where the blades are released from a frangible section at the root of the blades to prevent burst. Although the intention is to release the blades simultaneously, there is a possibility of a sequential blade loss. This is also called as "domino" sequence and this scenario is associated with the most severe unbalance loads. The total time between the first blade release and the last blade releasing is about 5 ms.

In gas turbine engines, generally three types of blade to disk connections are used. These are the dovetail, firtree and the blisk (bladed disk) arrangements. Dovetails are associated with cold section components like fans and compressors. Similarly, blisks are also widely used in modern engine compressors. Turbines operating at low temperatures also have blisk connections, i.e., micro gas turbines. An energy conservation turbine (steam turbine) for small cogeneration applications manufactured by ET Group features a stainless steel blisk. It is reported that this turbine can withstand over 150% speed which is higher than the blade release speed of similar applications. The material also allows 13% radial growth (30 mm) before failure which makes rotor to casing rub possible for overspeed prevention [8]). Despite the examples of blisk turbine rotors of several manufacturers, firtree connections are the dominant type in gas turbine hot section components [24,3,17].

1.2. Approach in current study

Fan blade-off is generally related to component life-related failures and is a widely studied phenomenon in aero engines [29,35]. Nevertheless, despite the applications in commercial engines, there are very few modelling studies in the open literature on turbine blade-off. This is the main motivation of the current research, and the focus is placed on developing an approach to release the blades by purpose at a predetermined speed to avoid disk burst.

The controlled blade-off reported herein relies on the behavior of the disk post and blade firtree at near-burst conditions. Following a parametric design approach, three main outcomes were observed by finite element simulations. These are the disk burst, blade escape from the disk post, and blade-off by disk post failure with intact firtree.

Modelling methodology

To conduct a design space exploration, a parametric blade retention system is used which is formed by a blade firtree and a disk post (Fig. 2-a). The serrations of the blade firtree form a recess and a protrusion to the disk post and this connection retains the blade during rotation. These serrations form a 'V-shape' at their point of contact defined by the angle 2.β (Fig. 2-b). Each serration is formed by an upper flank, a lower flank and a connection fillet (Fig. 2-c). During rotation, contact between the blade firtree and the disk post occurs at the regions of lower flank.

The blade parametrization has three parameters, and these are qualitatively described herein.

- The first parameter is the contact angle 2.β. The higher values of the contact angle are named as 'Opened-V' while the lower values are named as 'Closed-V'.
- The second parameter is the relative thickness of the blade firtree to the disk post. These are controlled with the parameters L_1 and L_2. So, the reference condition is called as 'thick' and the disk post having a lower value of parameter L_1 is called as 'thin'.
- The third parameter set is the length of the upper (L_3) and the lower (L_4) flanks. Reference conditions of these are indicated as 'long' and shorter versions are indicated as 'short'.

While making the serrations shorter, the lower flank is also rotated counter clockwise from its centre. The reason behind this is to facilitate blade escape with the radial growth of the disk at overspeed conditions. Two flanks are than bridged in the drawing programme to form the connection fillet which has a radius, R. These modifications are done at the mid-line and then the serrations are rotated counter clockwise at an angle of half contact angle β. These left-hand side serrations are then mirrored according to the mid-line to form the right-hand side serrations. It should be noted that the parametrization described herein does not form a parametric disk and blade system. The disk from bore to rim is the same and the blade above the firtree is the same as well. There are three parameters in the firtree parametrization which would be much higher in a study which concentrates on fine tuning a geometry. For example, Song et al. [31] carried out a firtree design optimisation study with 16 parameters and 16 variables. The reason for keeping the disk and blade the same and restricting the number of parameters with 3 is to concentrate on releasing the blade and explore whether a solution exists for overspeed protection or not.

The firtree attachments have been studied by many scholars and the stress state is case-dependent based on the presence of slip or stick, local gaps or contact loss. Following a stress-freezing experimental study, Meguid [22] studied an aero-engine blade firtree attachment with changing design parameters like flank angle, skew angle, and friction coefficient. As a general characteristic, two stress peaks, one at the contact region, and one following the end of contact occurred at similar magnitudes. Increasing flank angle (40 and 50 degrees) increased the peak stresses. At the mid-section of the disk post, increasing friction coefficient from 0 to 0.5 increased the stresses by 10% and increasing the friction coefficient from 0.1 to 0.5 increased the stresses by 2%. Papanikos et al. [25] studied a compressor dovetail joint and reported that disk stresses decrease with increasing friction coefficient for sliding contacts. For sticking contacts ($\mu > 1$), the stresses increased with friction coefficient due to contact separations at the upper parts of the contact interface. According to Zboinski [39], increasing the friction coefficient tends to decrease the stresses. However, the effect of clearance due to manufacturing or assembly deviations found to be substantially influential on the results with or without friction.

The intention of the parameterization is to identify whether there is a solution that results in the release of the blades at lower rotational speeds which can be used as a controlled parameter for burst prevention. According to the simulations, a solution space exists and there are three types of post terminal speed rotor behavior. These are given in Fig. 3. The first outcome is the disk burst which is associated with the long flanks (Fig. 3a). The long flanks retain the blades and the blades only disengage from the disk

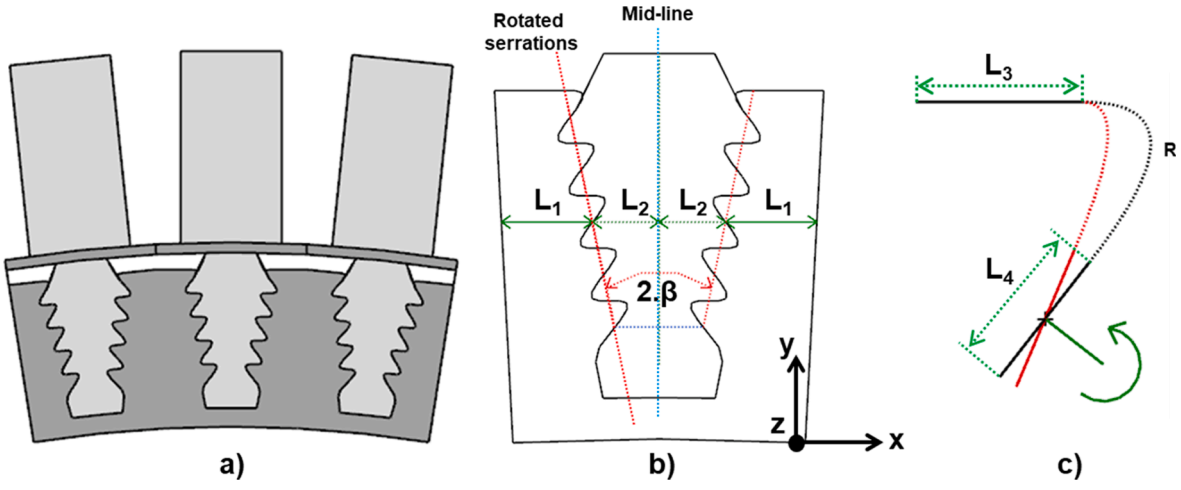

Fig. 2. Notional geometry describing firtree parametrization.

following the burst. The second type of behavior is the blade escape which is mainly associated with 'Opened-V', and short flanks (Figure-3b). In this case, local deformations in the serrations lead to the escape of the blades before the burst speed. The third type of the behavior is mainly related with 'Closed-V' (Fig. 3c). Different than the blade escape, in this case because of the fracture of the disk post, blades disengage from the disk before the burst speed.

A three-dimensional sectoral LS-DYNA model was prepared, and the results were compared against a full circumference, three-dimensional simulations (Figure-4a). Upon achieving agreement between these models, the low computational cost sectoral model was used for the design space exploration requiring a series of simulations with changing firtree geometries and boundary conditions. In the one-blade sectoral model with cyclic symmetry boundary conditions, the effect of the rotation was applied as a centrifugal load. On the other hand, in the full circumference model the rotation was applied via a rigid spinner that is attached to the upstream drive arm. It should be noted that a rigid component attached to the deformable rotor changes the terminal speed behaviour substantially. To avoid this effect, the rigid spinner and the upstream drive arm were adjusted to have a geared shape and a contact between these parts was defined (Fig. 4-a). With the increase in the rotational speed, the drive arm was able to deform naturally in the radial direction with the other parts. As a result, an agreement between the rotor tip displacement, speed and the type of terminal behaviour were achieved among the models. A cooled rotor disk temperature profile was used. For the blades, a gas temperature profile with a radial temperature distribution factor of 0.1 is assumed and the peak temperature is located at 60% blade span [32,20]. The gas temperatures were then scaled to metal temperatures. The temperature gradient was applied in the radial direction only, and the temperature distribution in the axial direction was assumed as uniform. The material was Inconel-718 and the Johnson-Cook constitutive and failure models were used in the simulations [18,21]. The geometry of interest and the boundary conditions reflect a modern turbofan engine where the operating conditions correspond to maximum continuous thrust at sea level. The results are normalized according to the reference condition and the relative changes of different geometries are plotted accordingly.

The simulations here correspond to the turbine rotor only. However, the turbine rotor is part of a global all-in-one turbine assembly simulation model including the upper casing, and the downstream stationary structures. For that reason, a minimum model size was targeted to avoid high computational cost. In Fig. 4-b, the simulation time of the single blade sector model is plotted as a function of the model size for three different types of mesh groups. The mesh size is associated to the increase in disk mesh but more dominantly the firtree mesh. In Group 1, the mesh size in the firtree serrations is 1 unit in the circumferential plane. In Group 2, the size is 0.7 units and in Group 3, it is 0.4 units. The skew angle of the disk slot is zero. The circumferential mesh is extruded in the axial direction (z-axis) resulting in different aspect ratios (AR). These aspect ratios are given for each case near the data points. So, for a given mesh group having the same density in the circumferential plane, a lower aspect ratio indicates high number of elements in the axial direction. The selected mesh used in the simulations is the M1 having model size of 1 unit and a simulation time of 1 unit. It is seen that an exponential increase in the simulation time occurs with the increasing model size.

It was observed that the stress distribution in the firtree serrations changes as a function of element size in the circumferential plane (x-y plane of Fig. 2). The effect of axial elements (z direction), which indicates the aspect ratio, was low. In Fig. 5, the normalized equivalent stress distribution of each firtree serration is plotted for M1, M2 and M3. These distributions correspond to the firtree mid-section and represent each mesh group. The plot starts with the first firtree protrusion (P-1) and this is followed by the contact (C-1) between the firtree and the disk post. There are two stress peaks in the contact region C-1-a and C-1-b. These are compressive in nature. This balanced stress distribution corresponds to the longer flanks with large bearing surfaces. Later, it was observed that the stress peaks converge to a large peak in the short flank serrations having less bearing surfaces in the design space. After the contact, the connection fillet starts which bridges the lower and the upper flanks. The lower part of this recess has another stress peak at R-1-a which is tensile and the stress peak after the recess turn at R-1-b is compressive. The upper flank region of the blade firtree which forms the protrusion to the disk side is a low stress zone.

Mesh M3, with the highest mesh density in the circumferential plane, provides a better resolution of the stress distribution peaks at the contact points from C-1 to C-5. It is also seen that they deviate from the M1 at the peak stress values of first (R-1) and the second

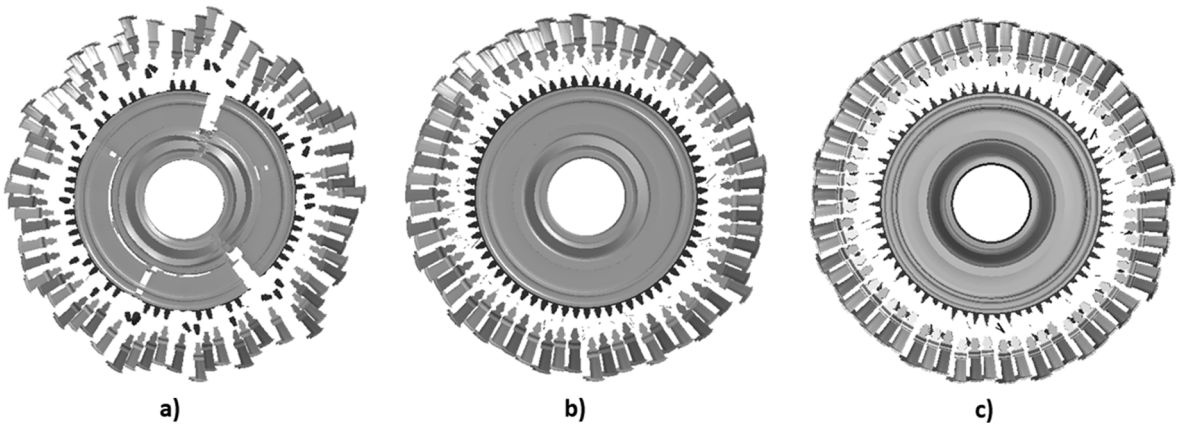

Fig. 3. Turbine rotor scenarios.

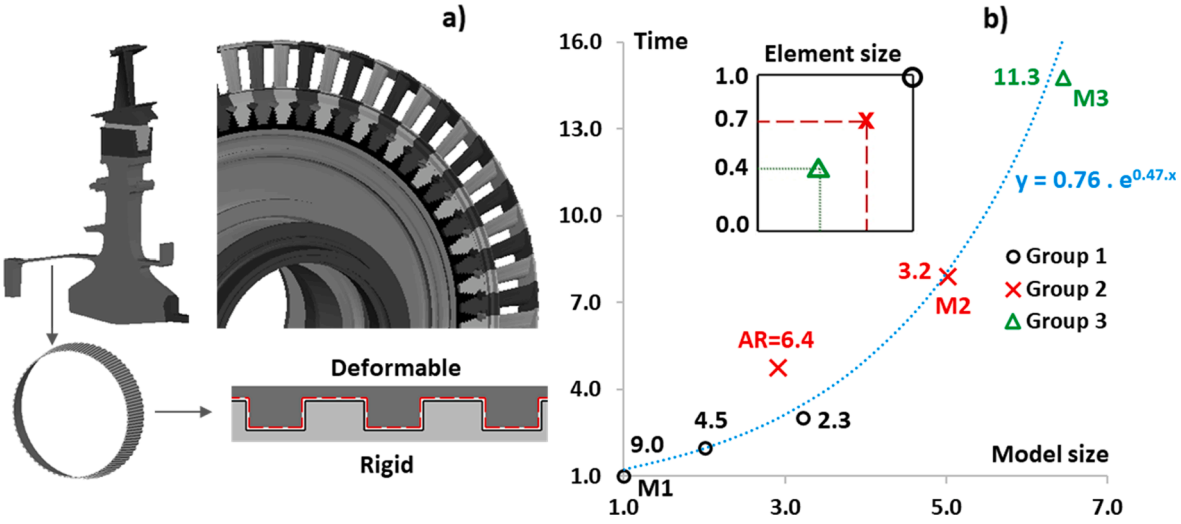

Fig. 4. Finite element models and the mesh density.

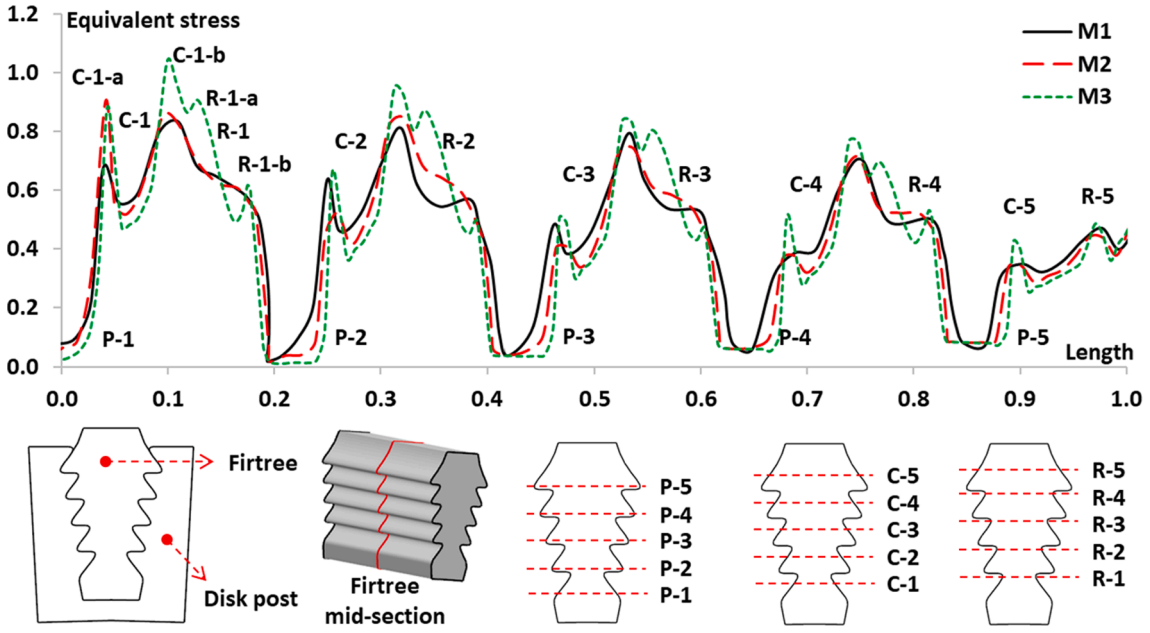

Fig. 5. Firtree stress distribution for different mesh groups.

recess (R-2). Despite these deviations of M1 and M2 from M3 at the two lowest serrations, they have a good generalisation capability. The terminal behaviour of the rotor, which was burst, and the terminal speed are the same for all mesh configurations. Same comparison was done for other extreme cases resulting in blade disintegration before burst, and the final outcome came out to be the same as well. For this reason, instead of using M2 (4 times longer time) or M3 (15 times longer time), M1 was used for the simulations. The full circumference model of the M1 also takes 10 times longer than the one blade sector model. So, using M2 or M3 was impractical from a computational cost point of view.

Design space exploration

By following the methodology discussed in the previous section, a design space exploration was carried out through successive simulations of the one-blade sector model. In Fig. 6, the design space is represented by four curves. The terminal rotor speed is plotted as a function of the contact angle. The top curve is the reference case with different contact angles. On the right-hand side of the design space featuring 'Opened-V', there are two outcomes. For long flanks, the outcome is disk burst and for short flanks the outcome is blade

escape. On the left-hand side, which is separated by a vertical line, disk post failure is seen for all cases. The centre region featuring 'Middle-V' has a mixed characteristic. Long flanks with thick disk post result in a disk burst. Long flanks with thin disk post result in disk post failure. Both short flank configurations here result in blade escape.

There are two mechanisms in the firtree and disk post attachment which lead to different terminal speed behaviour. The first one is the stress distribution at the serrations. In Fig. 7, the stress distributions of the short firtrees are plotted together with the reference case. The blunt serrations with shorter flanks have lower load bearing surfaces. This contributes to an increase in the stress. The increased contact angle, 'Opened-V' loads the upper serrations and unloads the lower serrations. 'Closed-V' acts in the opposite sense. Despite the unloading condition, due to the increased shear component in the 'Opened-V', the equivalent stresses are higher than the others. As a result of this, the blades slip and escape from their retention before disk burst. It is also seen that the multi-peak condition of the long flanks has changed to a single large peak in short flanks.

The second mechanism affecting the terminal speed is the stress distribution in the disk post. The thickness of the disk post in the 'Opened-V' is higher at lower serrations and lower at the higher serrations. On the other hand, the disk post thickness in 'Closed-V' has a more uniform thickness from bottom the top. Due to the relative reduction of the disk post thickness, for 'Closed-V', the disk post middle region is more affected by the stress state of the serrations. According to Fig. 8, it is seen that the stress values at the mid-section of 'Closed-V' is substantially higher than the 'Opened-V'. This condition is independent of the flank lengths, but the long flank serrations affect the disk post more as they penetrate more into the retention. The stress values are the highest for 'Closed-V' thin disk post and the presence of the serrations are visible with the wavy stress distribution. The highest stress occurs at the first and second serrations and the fracture of the disk post occur at this location which can also be seen at the left-hand side of the parametric design space of Fig. 6.

In summary, for the thick disk post, the combined effect of the 'Closed-V' and the blunt serrations is just enough to trigger disk post failure at a speed very close to the disk burst speed. The effect of thin disk post is more dominant in reducing the terminal speed as it appears around 1.3 speed units for thin configurations regardless of the flank configuration. This early blade-off is achieved at the expense of increased stresses especially at lower serrations. On the right-hand side of the design space, the blade escape of 'Opened-V' occurs at 1.43 speed units, which is quite close to the disk burst speed.

3.1. *Effect of contact friction coefficient*

The right-hand side of the design space with the 'Opened-V' contact angles is associated with the escape of the blades following the local deformation of the blunt serrations. Therefore, it is worth to investigate the effect of the contact friction coefficient at the serrations of the blade firtree and the disk post to see how the design space changes in terms of the terminal speed and the outcome.

Various contact friction coefficients for blade retention systems are used in literature ranging from low to high friction coefficients. For example, in gas turbine blade attachments, Yu et. al. used the value of 0.15, Pande et. al. used the value of 0.3 and Witek & Stachowicz used the value of 0.05 [38,26,36]. At low contact friction coefficients, the mating surfaces are prone to slip which results in

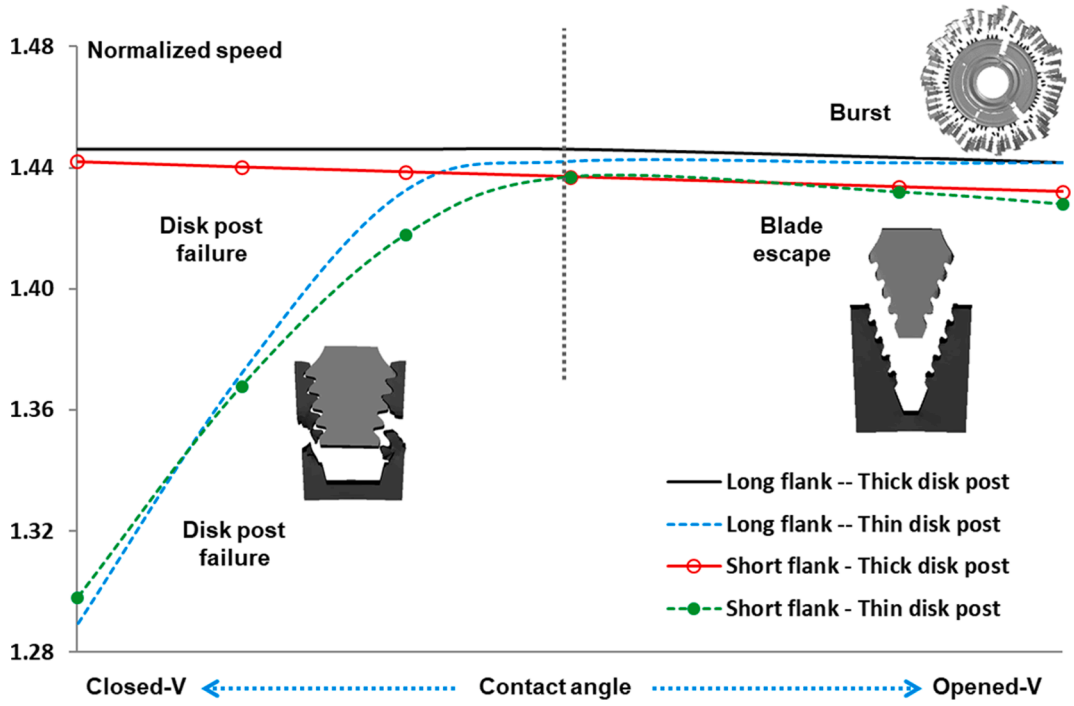

Fig. 6. Design space.

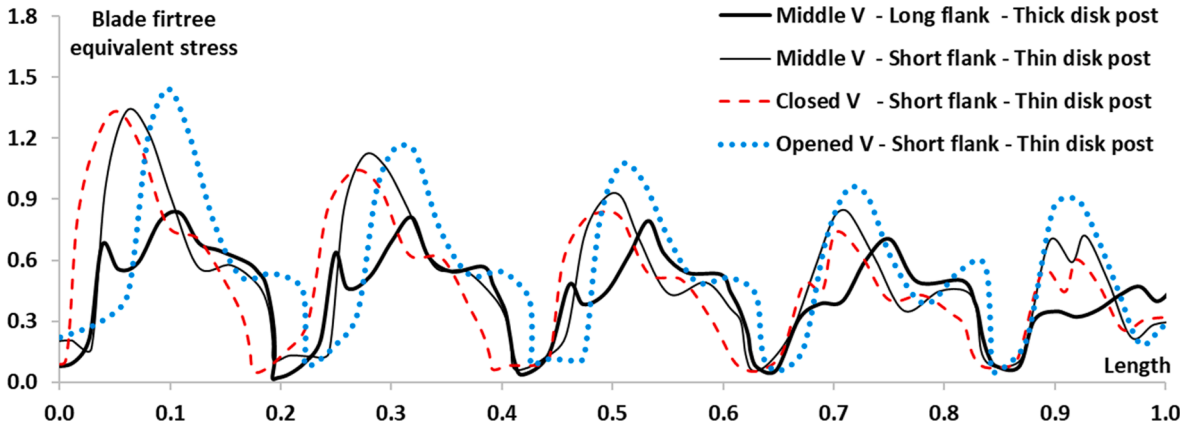

Fig. 7. Stress distribution of serrations.

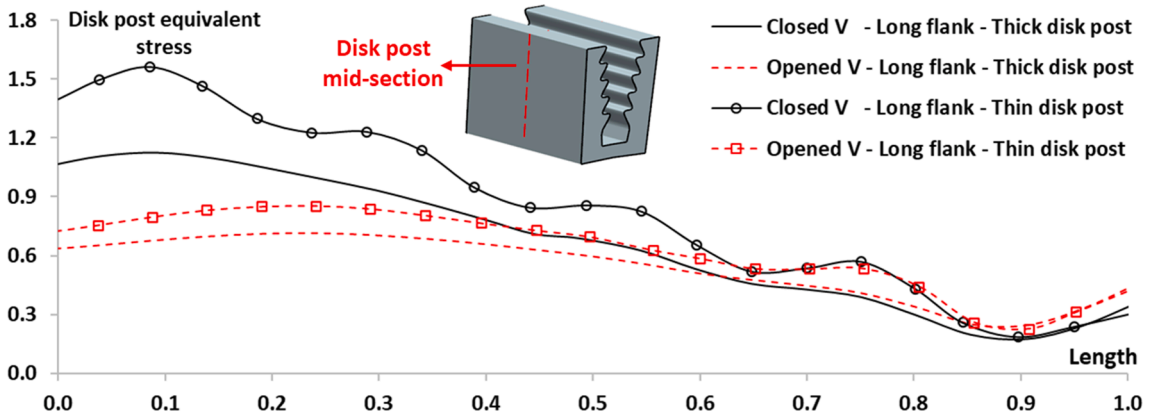

Fig. 8. Stress distribution of the disk post.

fretting. This relative movement reduces the component life. Shim et al. [33] reported an experimental friction coefficient value of 0.6 for bare nickel disk alloy and NiCrMnSi coated disk alloy. To improve the wear resistance of the firtree attachment, an oxide layer coating was proposed. The experimental results of the SiO_2 coated nickel disk alloy were reported to be 0.52.

For this study, the friction coefficient is 0.1 and the design space for the value 0.5 is plotted in Fig. 9. It was observed that the high friction coefficient shifts the design space upwards, this becomes most visible for the blunt serrations and thin disk post configurations. The design space with 0.1 friction coefficient moves upwards around 2% at the right-hand side and moves upwards around 5% at the left-hand side. For 'Closed V', there is still a 10% margin to the disk burst speed.

Friction coefficient has a direct effect on the relative movement between the blade and the disk. This is defined as slip, and this changes the contact interface. In Fig. 10, the effect of friction coefficient on the slip is given for the lowest blade serration with respect to the disk post serration. Slip decreases with increasing friction coefficient and the long flanks have less slip than the blunt flanks. In terms of the contact angles, 'Opened V' indicates higher slip. The value of the 'Middle-V', long flank and the thick disk post at 0.1 friction coefficient has a slip value of 1 unit. Compared to this value the effect of flank angle and the bluntness is significant.

At high slip, flank-to-flank contact interface reduces because the blade side flank slides over the disk side flank and moves towards the connection arc of the disk side serration. This increases the stress intensity of the contact. At high friction coefficient flank-to-flank interface becomes longer and the stress levels reduce due to increasing load bearing surface between the mating parts. This is shown in Fig. 11. Increased friction coefficient loads the lower serrations and unloads the upper serrations. Despite this condition, the stress level at the lower serrations still reduces. At low slip, which is below 1 unit, it was observed that there is a slight increase in the contact stresses, but this increase is less. The disk post mid-section stresses also reduce. The primary reason for this is associated with the lowering stresses in the serrations. The secondary reason is associated with the reduction of the blade centre of gravity at less slip. However, the effect of the latter is lower. As a result of the reduced stress levels, the firtree sections enter the plastic deformation later and the design space of Fig. 9 shifts upwards.

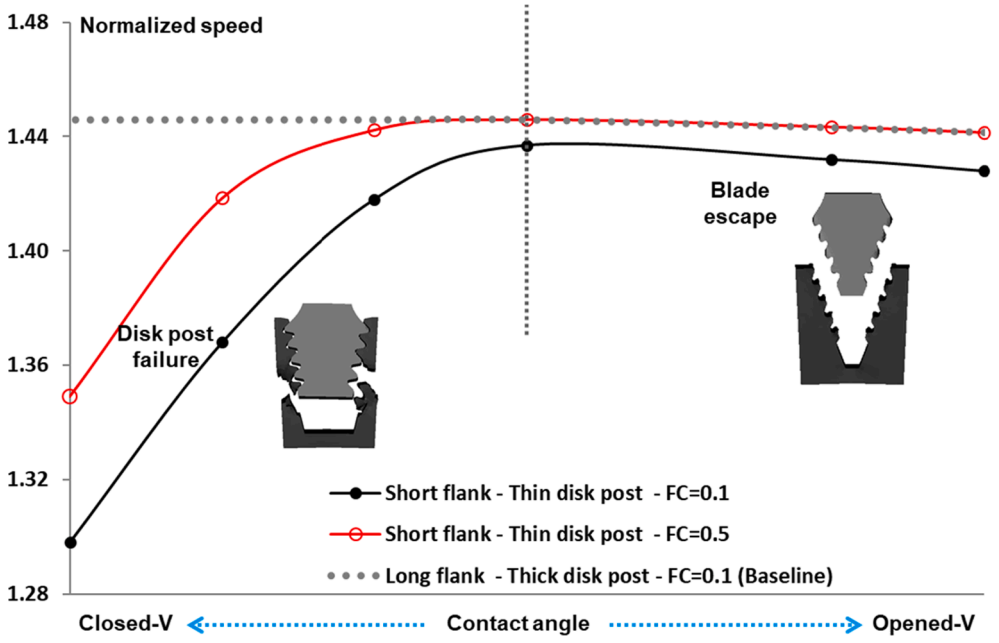

Fig. 9. Effect of the friction coefficient on design space.

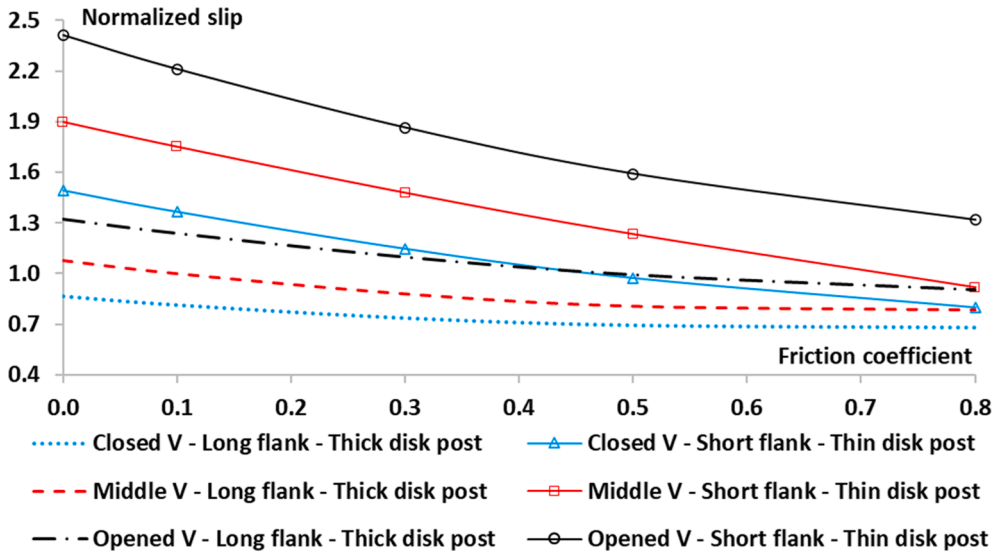

Fig. 10. Effect of friction coefficient on slip.

3.2. Effect of serration number

The parametrized firtree has five serrations and to investigate the effect of the number of serrations, the lowest firtree contact was cancelled. While doing this, the lowest serration was still attached to the blade, so the total mass and the centrifugal load of the blade was the same. When the four serrations share the total load of the initial five serrations, the blade-off speeds go down. For short and long flanks, the terminal speed shifts 6% down for 'Closed-V'. For 'Opened-V' the long flank terminal speed does not change but the short flank terminal speed reduces significantly (Fig. 12). Similar significant reductions occur at the Middle-V as well. At 'Middle-V' configuration, the terminal behaviour at this region was 'burst' or 'blade escape' for long flanks, but for 4 serrations the terminal behaviour is 'disk post failure'. So, the limit shifts towards higher contact angles. But for short flanks the limit is the same and the transition from 'blade escape' to 'disk post failure' occurs at the 'Middle-V'.

For the thick disk post configurations with long flanks, the terminal speed and the final outcomes didn't change with the reduction of the serrations. Only for 'Closed-V', the disk post failure occurs around 1% sooner. This is the same for the blunt flanks as well. For the

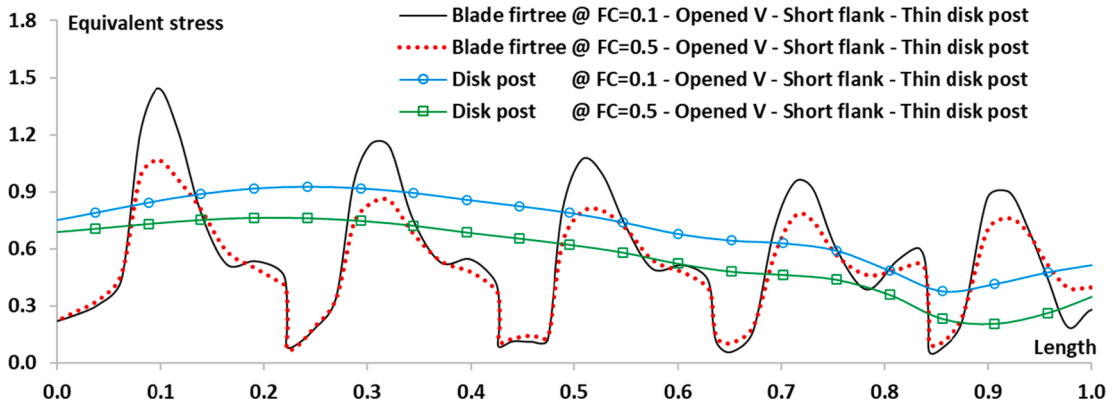

Fig. 11. Effect of the friction coefficient on stress.

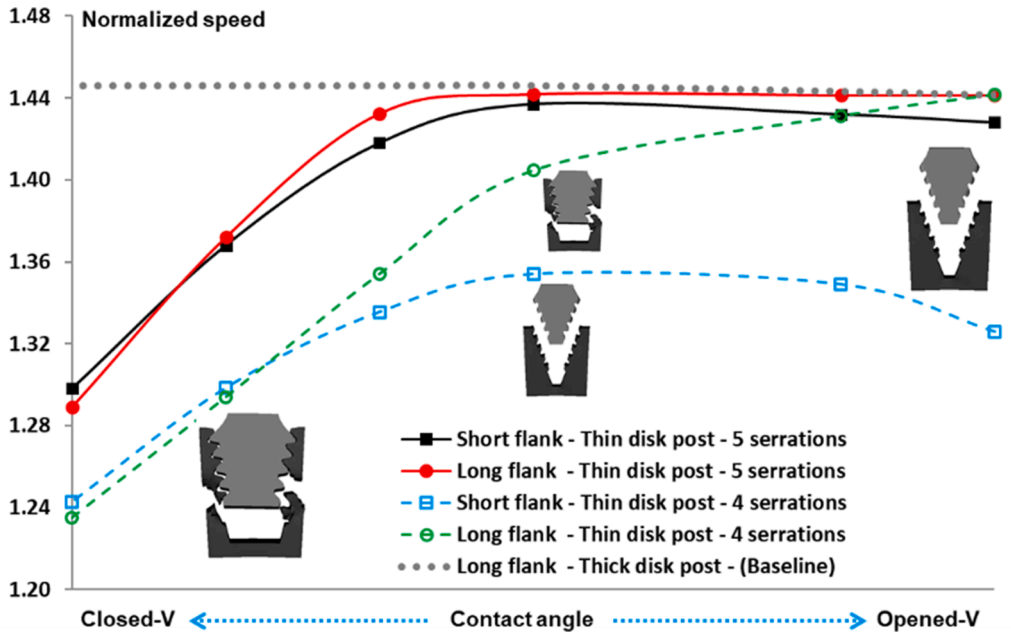

Fig. 12. Effect of serration number.

'Opened-V', the blunt serrations with thick disk post show a similar behaviour with the thin disk post versions and the blade escape occurring around 6% lower than before.

3.3. *Effect of blade tip displacement*

The containment of the blades for a simultaneous turbine blade-off during an overspeed was previously studied by Eryilmaz and Pachidis [5]. It was observed that the required casing thickness increases with the number of blades being lost at the same time. In that study, the casing was placed at a higher radius and the effects of blade to casing rubs prior to the blade-off were ignored. The same assumption is still valid in the current study as there is no casing at all in the simulations. However, before the terminal speed, there is a possibility of blade to casing rub. This was investigated together with different strain hardening properties of the material, and the tip displacements were monitored for possible rotor to casing rub prior to the terminal speed. The Johnson-Cook constitutive model is given in Equation (1) [18,21]. For the high strain hardening curve, the B parameter is set to be 95 MPa higher than the reference value and the n parameter is set 0.15 lower than the reference. For low strain hardening, the B parameter is 65 MPa lower than the reference and the n parameter is 0.3 higher. The elastic part is kept constant to ensure the models exceed the yield limit at the same loading.

$$\sigma = \left[A + B.\epsilon_p^n\right].\left[1 - \left(\frac{T - T_{room}}{T_{melt} - T_{room}}\right)^m\right].\left[1 + C.\ln\frac{\dot{\epsilon}}{\epsilon_o}\right] \quad (1)$$

Decreased strain hardening indicates more disk plastic growth after the yield and more plastic deformation before fracture. Increased strain hardening indicates more brittle behaviour. This allows the material to withstand higher loads but has less plastic deformation before fracture. While changing the strain hardening parameters, the damage parameters of the material model were kept the same. This resulted in almost the same blade tip displacement (overall plastic growth in the assembly). For that reason, different strain hardening parameters have all shifted the design spaces regardless of the geometric parameters. For the high strain hardening case, the terminal speeds are 6% higher and for the low strain hardening they are 3% lower than the initial design space.

For all designs, the blade tip displacements follow the same curves which are given in Fig. 13-a as a function of the rotational speed. The starting point of the horizontal axis corresponds to the speed where the rotor tip clearance becomes zero. This is named as Scenario 1 in Fig. 13-b. After the rotor consumes the tip clearance during the overspeed, rotor to casing rub start. According to Scenario 2, the erosion of the rotor and the casing are equal. In Scenario 3, only the casing liner is eroded and in Scenario 4, the casing is intact and only rotor material erodes. In a real case condition, the casing liner is weaker to compensate nominal operation rubs, so a combination between Scenario 2 and Scenario 3 should be expected. According to Scenario 2, the rotor knife edge tip seals and the same amount of casing liner are eroded in Region 1 of Fig. 13-a. In Region 2, rotor shroud and the same amount of casing is lost. In Region 3, the rotor blades start to rub to the casing. The Point P_1 represents the 'Middle-V', long flanks and the thick disk post case resulted in disk burst. Point P_2 represents the 'Closed-V', short flanks and the thin disk post case which was resulted in disk post failure. Point P_3 is the 'Opened-V', short flanks, and the thin disk post where the outcome was blade escape.

Prior to Point P_1, the rotor loses tip seals and the shroud. This mass loss delays the terminal speed and friction can also save time for the control system to act. However, there is little difference in the speeds of Region 2 and Region 3 for a given strain hardening curve, which are almost a flat line. Due to the very short and indeterministic nature of the event, the shortcoming of Point P_1 is that the rotor may inhibit premature burst because of the defects or deformations which may accumulate during the life cycle. Point P_3 gives a 3% blade-off margin and features blade to casing rub. Point P_2 gives about 15% blade-off margin but the rub is minimal.

Discussion and further considerations

How fast a rotor accelerates, and how high its speed can go up to, is a function of three parameters in general. The first one is the engine's aero-thermodynamic performance. This includes the amount of gas being expanded through the turbine during the gas blow down from the combustor, and the number and magnitude of the compressor surge and recovery cycles that may lead to continuous air flow. The second one is how long it takes to detect overspeed and shut the fuel flow. The third parameter is the rotor inertia. A combination of the above three conditions, as well as mechanical considerations in the form of friction or controlled blade-off, define the terminal speed. A terminal speed leading to a hazardous condition which cannot be contained within the engine's casing is not certifiable.

In this study, the parametric design space exploration keeps the total mass of the blade firtree and disk post almost the same and within a 1.5% maximum variation. For this reason, the maximum speed that the disk can withstand (burst speed) remains almost constant throughout the design space. The changing parameter in the design space is the terminal speed which the system may experience. This could lead to a disk burst which is not certifiable. Alternatively, the terminal speed can lead to a blade-off scenario which may be certifiable, provided that the released blades can be contained within the casing. Of course, a terminal speed may be reached that does not lead to a disk burst or blade release due to some other preventative measure (e.g. fuel shut-off). The last scenario was not within the focus of this study, as the design space explored for various terminal speeds was generated from a mechanical perspective.

Regarding the finite element methodology, in the full circumferential model, the rotation effect would be implemented by a centrifugal force however the rotor was rotated instead as the model was a part of all-in-one whole model to investigate the effects of conditions such as casing containment capacity, sequential loss of blades due to unintentional failure of single blade and the unbalance loads. In engine, the blades rotate with the effect of the gas pressure that flows through the stage. Here instead, a rigid spinner was used and care should be taken while using this kind of arrangement. If the rigid spinner is attached to the deformable rotor through merged nodes, the deformations and hence the burst or final speed of the rotor changes. Therefore, the geared shape of the spinner for rotation through a contact allowed the deformable rotor assembly to grow in the radial direction naturally.

A summary of the findings is given in Table 1. Considering the 'level' of speed the system can attain, blade-off speed should not be too close to the nominal speed, (this would indicate even higher stress levels during nominal operation) and should not be too close to disk burst either. This is important to guarantee the release of the blades during an overspeed event because of its fast and indeterministic nature. In this study it was observed that a contact angle forming a 'Closed-V' results in disk post failure at a low rotational speed, providing a healthy margin between blade-off and burst speeds. Blunt firtree serrations make the blade firtree prone to disengage from the disk post and release before burst. But the margin between blade-off and burst speeds is low.

Slip between firtree and disk post reduces with increasing friction coefficient, the stress levels decrease, and the margin between the release speed and the burst speed reduces. From a controlled blade-off perspective, this is an adverse effect. With the reduction of the serration number, it was observed that the right-hand side of the design space, 'Opened V', becomes more responsive to the design changes. The margin between the disk burst speed and the blade-off speed becomes higher in this case.

The shape of the design space does not change with the change in strain hardening behavior. Low strain hardening starts the plastic growth of the disk earlier which is beneficial with respect to rubbing and friction torque generated between blade shrouds and the casing. However, this also reduces the margin between the nominal speed and the disk burst speed because the disk capability is lower in this case. For a fast overspeed, due to engine and rotor properties, and the possibility of a premature disk burst, another viable option is to use a brittle material represented by high hardening. A high strain hardening behavior increases the speed that the disk can

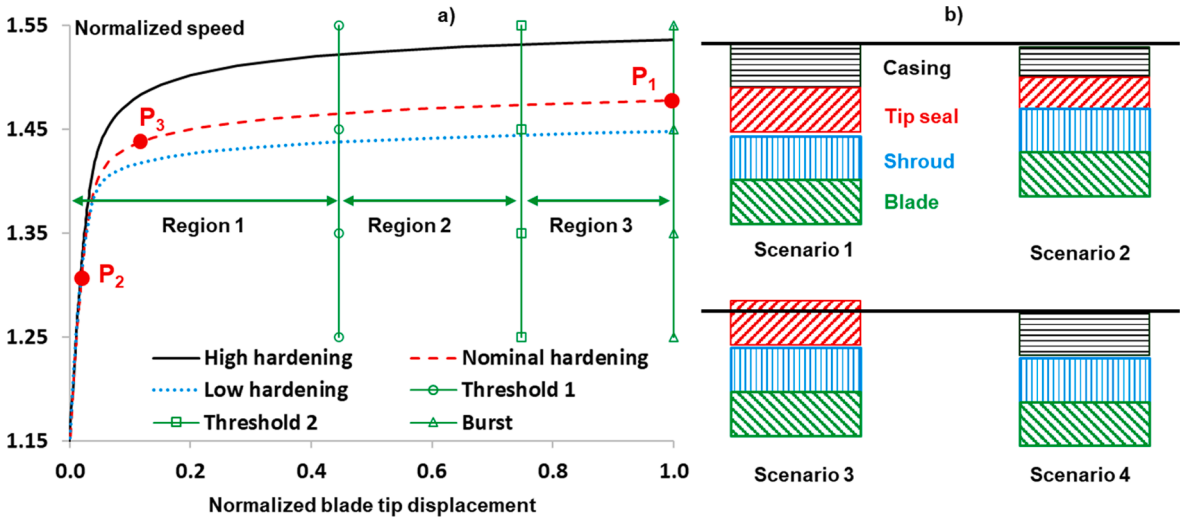

Fig. 13. Effect of blade tip displacement.

Table 1
Summary of the outcomes.

Flank length	Disk post thickness	Contact angle
Reference	Reference	Closed-V: Outcome is disk-post failure. Mid-V: Outcome is disk burst Opened-V: Outcome is disk burst
Reference	Reduced	Closed-V: Outcome is disk-post failure. Mid-V: Outcome is disk-post failure. Disk burst at high friction coefficient. Opened-V: Outcome is disk burst
Reduced	Reference	Closed-V: Outcome is disk-post failure. Mid-V: Outcome is blade escape. Disk burst at high friction coefficient. Opened-V: Outcome is blade escape.
Reduced	Reduced	Closed-V: Outcome is disk-post failure. Mid-V: Outcome is blade escape. Opened-V: Outcome is blade escape. Disk burst at high friction coefficient.

withstand. In this case the plastic deformation would be less, with a possible failure at the end of Region 2, but the delayed burst and the friction at Region 1 could save the disk from bursting. But in any of the hardening conditions, there is still a gap between the release speed and the burst speed where the contact angle forms a 'Closed V' at the left-hand side of the design space.

It is acknowledged that certification for blade shedding requires a very careful 'accounting' of the combined effects of material properties, operating temperatures, and manufacturing tolerances [11]. In this study the focus has been on the exploration of a firtree-based design space. Aforementioned factors were not considered in the modelling in any great detail. For example, the temperature gradient in the assembly was defined in the radial direction only, and not in the flow direction, as a simplification. This would have an impact on overall rotor behavior and the firtree regions. Cooling flows are fed to the rotor mainly from the upstream rim which is close to the firtree. These can change local material strength and failure conditions. Another operational factor is stress variations among different geometries in the design space. The design space has variations in the slip between the blade firtree and the disk post. There are also changes in the stress levels from one design to another. Therefore, a low cycle and high cycle fatigue assessment would have been helpful.

Moreover, blades are generally manufactured from single crystal castings. On the other hand, the raw material of the disks can be in the form of powder, cast, wrought or forged. Without loss of generality, it was reasonable to assume the same material for the purposes of this academic study. But, in practice, there are variations in the material properties. Another factor is the manufacturing of the contact surface. Firtree serrations have very high-quality surface finish. This is traditionally obtained by a broaching process or by electric discharge machining. These manufacturing processes have tolerances of around 10–20 μm and the firtree serrations can be considered as uniform around the circumference. Nevertheless, firtree fixing is a dynamic process where a small relative motion between the blade and disk occurs. For that reason, stresses are not even and the parts wear around the circumference. Due to these local variations around the circumference, achieving simultaneous blade loss becomes more difficult. Apart from the firtree region, it should also be noted that other parts, including the disk and the blades, are subjected to uneven distributions of stress in service. This is also not considered in the current study.

Conclusions

This work explores the possibility of blade failure as a control mechanism for turbine overspeed by focusing on a single turbine stage. The design space search is conducted by parametrizing the blade firtree and the disk post. The parametrization was based on the firtee contact angle, flank lengths and the thickness distribution between the blade firtree and the disk post. According to the simulations, it was observed that a design space for this purpose exists, especially for low contact angles with reduced disk post thickness. The increased stresses in the disk post trigger failure at a speed lower than the disk burst speed. Another possibility of controlled blade-off is associated with the blunt serrations leading to the escape of the blades. But in this case, the blade-off speed and the disk burst speed are quite close to each other. In all scenarios, blade-off became possible with increased stress levels at nominal operation.

Stress levels are also a function of the friction coefficient. Slip is lower at increased friction coefficient, and this reduces stress levels. Less relative motion between blade and the disk is also beneficial in reducing fretting. This is a desired condition for nominal operation but acts in the opposite sense from an overspeed prevention perspective.

The strain hardening parameter needs to be carefully considered together with engine aero-thermodynamics and rubbing between shroud and the casing. A low strain hardening rotor indicates earlier friction generation, but if the overspeed time evolution is very aggressive for a turbine stage, it is more desirable to select a high strain hardening rotor with higher disk burst capability to allow more time for the engine control system to react.

The methodology presented in this paper and the obtained design space provide a guideline for the selection of design parameters for simultaneous blade release at a predetermined rotational speed for disk burst prevention. Provided that simultaneous blade release can be ensured, and debris contained in the system via the use of a stronger casing, blade-shedding can be an effective way to prevent disk burst since the gas torque acting on the rotor can be suddenly stopped.

Declaration of Competing Interest

The authors declare that they have no known competing financial interests or personal relationships that could have appeared to influence the work reported in this paper.

References

[1] Australian Transport Safety Bureau-ATSB: In-flight engine shut down involving Airbus A330-302 B-18358, Australia (2015). https://www.atsb.gov.au/publications/investigation_reports/2013/aair/ao-2013-172/.
[2] Australian Transport Safety Bureau-ATSB: Uncontained engine starter failure, General Electric CF6-80E1-A3, Australia (2008). https://www.atsb.gov.au/publications/investigation_reports/2007/aair/ao-2007-052/.
[3] Borufkafrank, H. P., Stiehler, F., Arrieta, H. V., Prokopczuk, P., Lorenzet, J.: Integrally bladed rotor disk for a turbine, US Patent 8821122 B2 (2014). https://patents.google.com/patent/US8821122B2/en.
[4] D.A. Cendon, B. Erice, F. Galvez, V. Sanchez-Galvez, Numerical simulation of tangling in jet engine turbines, International Journal of Turbo Jet Engines 29 (2012) 29–282, https://doi.org/10.1515/tjj-2012-0018.
[5] I. Eryilmaz, B. Guenchi, V. Pachidis, Multi-blade shedding in turbines with different casing and blade tip architectures 87 (2019) 300–310, https://doi.org/10.1016/j.ast.2019.02.025.
[6] I. Eryilmaz, V. Pachidis, Turbine thermomechanical modelling during excessive axial movement and overspeed, Aeronaut. J. 123 (260) (2019) 248–264, https://doi.org/10.1017/aer.2018.162.
[7] I. Eryilmaz, L. Pawsey, V. Pachidis, Multidisciplinary methodology for turbine overspeed analysis, Aeronaut. J. 122 (1257) (2018) 1711–1733, https://doi.org/10.1017/aer.2018.100.
[8] ET Group Turbine Technology: Blisk design, Retrieved 2 December 2020, https://www.etgroup.nl/en/blisk-design/.
[9] European Aviation Safety Agency-EASA: Certification specifications and acceptable means of compliance for Engines CS-E, Amendment 4 (2015). https://www.easa.europa.eu/sites/default/files/dfu/CS-E%20Amendment%204.pdf.
[10] European Aviation Safety Agency-Easa: Turbine over-speed resulting from shaft failure comment response document, CM-PIFS-003 Issue 01 (2012). https://www.easa.europa.eu/sites/default/files/dfu/certification-docs-certification-memorandum-EASA-Proposed-CM-PIFS-003-Issue-01_CRD_PUBL.pdf.
[11] Federal Aviation Admisnistration – FAA: Engine and Turbosupercharger Rotor Overspeed Requirements of 14 CFR - 33.27, ANE 111, US Department of Transportation (2011). https://www.faa.gov/regulations_policies/advisory_circulars/index.cfm/go/document.information/documentID/1019347.
[12] Frola, C., Vassallo, A.: Degiovanni, M., Mattone, M., Turbine clashing transient analysis: Impact of rotor disk stage onto static vane stage after shaft rupture, ASME GT2008-50216, Germany, (2008). 10.1115/GT2008-50216.
[13] A. Gonzalez, V. Pachidis, On the numerical simulation of turbine blade tangling after a shaft failure, ASME GT2014-27061, Germany (2014), https://doi.org/10.1115/GT2014-27061.
[14] M. Haake, R. Fiola, S. Staudacher, Multistage compressor and turbine modelling for the prediction of the maximum turbine speed resulting from shaft breakage, J. Turbomach. 133 (2) (2009), 021022, https://doi.org/10.1115/1.4001188.
[15] M. Herran, H. Chalons, D. Nelias, R. Ortiz, Prediction of engine mounting loads in transient dynamic response under blade shedding unbalance, ASME-GT2009-59615, Florida, US (2009), https://doi.org/10.1115/GT2009-59615.
[16] J. Hong, P. Yu, D. Zhang, Z. Liang, Modal characteristics analysis for a flexible rotor with non-smooth constraint due to intermittent rub-impact, Chin. J. Aeronaut. 31 (3) (2018) 498–513, https://doi.org/10.1016/j.cja.2018.01.003.
[17] Jankovec, J.: Optimization of turbine blade firtree root geometry using LS-Prepost in pre and post processing, 10th European LS-DYNA Conference, Wurzburg, Germany, (2015). https://www.dynamore.de/en/downloads/papers/2015-ls-dyna-europ.
[18] Johnson, G., Cook, W.: Fracture characteristics of three metals subjected to various strains, strain rates temperatures and pressures, Engineering Fracture Mechanics, 21 (1), (1985). https://www.sciencedirect.com/science/article/pii/0013794485900529.
[19] Lecuyer, D. J., Shapiro, A.: Turbine blade for gas turbine engine, US Patent 20150247419 A1 (2015). https://patents.google.com/patent/US20150247419A1.
[20] A.H. Lefebre, Gas turbine combustion, CRC Press, 1999.
[21] Livermore Software Technology Corporation – LSTC: LS-DYNA R7.1 Keyword user's manual Material Models, Volume 2, Revision 5442, Livermore, California (2014).
[22] S.A. Meguid, P.S. Kanth, A. Czekanski, Finite element analysis of fir-tree region in turbine discs, Finite Elem. Anal. Des. 35 (4) (2000) 305–317, https://doi.org/10.1016/S0168-874X(99)00072-4.
[23] National Transport Safety Bureau-NTSB: Aviation Accident Report, ERA14TA096 (2014). http://www.kathrynsreport.com/2017/02/eurocopter-as-350b3-ecureuil-united.html.

[24] Newman, A. J.: Turbine blisk, US Patent 7431564 B2 (2008). https://patents.google.com/patent/US7431564B2/en.
[25] P. Papanikos, S.A. Meguid, Z. Stjepanovic, Three-dimensional nonlinear finite element analysis of dovetail joints in aeroengine discs, Finite Elem. Anal. Des. 29 (3–4) (1998) 173–186, https://doi.org/10.1016/S0168-874X(98)00008-0.
[26] S. Pande, A.K. Pal, R. Pant, Stress Analysis and Study of Fir-Tree Assembly of Turbine Disc, International Journal of Current Engineering and Technology 6 (4) (2016).
[27] L. Pawsey, D.J. Rajendran, V. Pachidis, Characterisation of turbine behaviour for an engine overspeed prediction model, Aerosp. Sci. Technol. 73 (2018) 10–18, https://doi.org/10.1016/j.ast.2017.11.037.
[28] J.M. Pereira, B.A. Lerch, Effects of heat treatment on the ballistic impact properties of Inconel 718 for jet engine fan containment applications, Int. J. Impact Eng. 25 (8) (2001) 715–733, https://doi.org/10.1016/S0734-743X(01)00018-5.
[29] P.A. Roy, S.A. Meguid, Containment of blade shedding in gas turbine engines: part II—experimental and numerical investigations, Int J Mech Mater Des 17 (2021) 13–24, https://doi.org/10.1007/s10999-020-09516-8.
[30] Soupizon, J.: Device for limiting turbine overspeed in a turbomachine, US Patent 7484924B2 (2009). https://patents.google.com/patent/US7484924B2.
[31] W. Song, A. Keane, J. Rees, A. Bhaskar, S. Bagnall, Turbine blade fir-tree root design optimisation using intelligent CAD and finite element analysis, Comput. Struct. 80 (24) (2002) 1853–1867, https://doi.org/10.1016/S0045-7949(02)00225-0.
[32] F.M. Simpson, A rapid approximate method of determining axial flow turbine disk and blade temperatures, ASME Gas Turbine conference, USA (1967), https://doi.org/10.1115/67-GT-14.
[33] Shim, S., Bolcavage, A., Helmink, R. C.: Coating system including diffusion barrier layer including iridium and oxide layer, US Patent US 9689069 B2 (2017). https://patents.google.com/patent/US9689069B2/en.
[34] Transportation Safety Board of Canada: Aviation investigation report A08C0108, Engine power loss Canadian North Boeing 737-217, Canada (2018).
[35] N. Wang, C. Liu, D. Jiang, Prediction of transient vibration response of dual-rotor-blade-casing system with blade off, Proceedings of the Institution of Mechanical Engineers, Part G: Journal of Aerospace Engineering. 233 (14) (2019) 5164–5176, https://doi.org/10.1177/0954410019839884.
[36] L. Witek, F. Stachowicz, Thermo-mechanical stress analysis of the turbine of helicopter engine, Rzeszow University of Technology, Mechanika 88 (2016) 379–387.
[37] Y. Yang, Y. Xu, Y. Yang, D. Cao, Dynamics characteristics of a rotor-casing system subjected to axial load and radial rub, Int. J. Non Linear Mech. 99 (2018) 59–68, https://doi.org/10.1016/j.ijnonlinmec.2017.10.023.
[38] D. Yu, F. Li, J. Yang, K. Cheng, W. Shu, K. Lv, M. Li, Structural Optimization of Fir-Tree Root and Groove for Turbine Blade with Splines and Genetic Algorithm, ASME-GT2016-56518, Seoul, Korea (2016), https://doi.org/10.1115/GT2016-56518.
[39] Zboinski, G.: Physical and Geometrical Non-Linearities in Contact Problems of Elastic Turbine Blade Attachments, Proceedings of the Institution of Mechanical Engineers, Part C: Journal of Mechanical Engineering Science, 209(4), pp 273-286 (1995). 10.1243/PIME_PROC_1995_209_154_02.